Carbohydrate Polymers 349 (2025) 122963

Contents lists available at ScienceDirect

Carbohydrate Polymers

journal homepage: www.elsevier.com/locate/carbpol

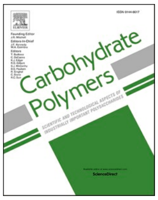

Biodegradable, robust, and conductive bacterial cellulose @PPy-P macrofibers as resistive strain sensors for smart textiles

Zaixian Yuan [a], Hai Yin [a], Min Zheng [a], Xiao Chen [a], Wei Peng [a], Hongfu Zhou [a], Jun Xing [a], Li Wang [b], Sanming Hu [a,*]

[a] *School of Biomedical Engineering and Imaging, Xianning Medical College, Hubei University of Science and Technology, Xianning 437100, PR China*
[b] *Wuhan Branch of the National Science Library, Chinese Academy of Sciences, Wuhan 430071, China*

ARTICLE INFO

Keywords:
Bacterial cellulose
Polypyrrole
Biodegradable conductive macrofibers
Resistive strain sensors
Movement monitoring

ABSTRACT

Fiber-based resistive strain sensors have attracted significant interest in the development of smart wearable devices due to their portability, flexibility, and easy conformability. However, current fiber-based resistive strain sensors mainly composed of metals and nondegradable polymers are not environmentally friendly and have poor mechanical strength. In this work, we examined biodegradable, robust, and conductive macrofibers fabricated through the in situ polymerization of p-toluenesulfonic acid (P-TSA)-doped polypyrrole (PPy) in bacterial cellulose (BC) nanofibers using wet-stretching and wet-twisting methods. The BC/PPy-P macrofibers possessed excellent conductivity (~7.19 S/cm), with superior mechanical properties (~210 MPa tensile strength and 2 GPa Young's modulus). Importantly, the BC/PPy-P microfiber operating as a resistive strain sensor possessed fast response time (15 s) and long-term stability (up to 1000 cycles), which could be used to effectively detect human movements. Moreover, the matrix material BC of BC/PPy-P macrofibers could be completely degraded within 96 h in the cellulase solution, leaving only PPy-P particles that could be recycled for other use. Therefore, the prepared BC/PPy-P microfibers provided a promising strategy for developing green resistive strain sensing fibers, with great potential to design eco-friendly smart fabric for monitoring human movements.

1. Introduction

As the basic unit of fabrics, fibers play a decisive role in the performance of fabrics. Recently, a large number of researchers have focused on the preparation of sensing fibers to design functional fabrics for personal movement monitoring (Dong et al., n.d.; He et al., 2019; Lin et al., 2017; Meng et al., 2018; Wang, Wang, et al., 2018). Among these, research on strain sensing fibers is the most mature and has been commercially applied. Strain sensing fibers used to construct functional fabric for monitoring mechanical movement mainly includes resistive (Dang et al., 2024), capacitive (Ma et al., 2021), piezoelectric (Qian et al., 2023), triboelectric (Fan et al., 2020), and electromagnetic fibers (Du et al., 2020). Resistive strain sensing fibers enable human movement monitoring through resistance changes of conductive fibers in response to external forces, which have the advantages of a simple structure, low preparation cost, and easy construction of functional fabrics compared to other types of sensing fibers (Lee et al., 2021; Souri et al., 2020). Therefore, numerous studies have been conducted on conductive fibers as resistive strain sensors.

Conductive fibers for resistive strain sensing fibers mainly include metal-based fibers (Liu, Miao, et al., 2022), carbon-based fibers (Li, Ni, et al., 2022), conductive polymer-based fibers (Song et al., 2024), and hydrogel-based ionic conductive fibers (Wang et al., 2022). Metal materials such as metal wires, metal nanoparticles and nanowires, and liquid metals are considered very attractive for the preparation of conductive fibers due to their excellent electrical conductivity (Liu, Zhu, et al., 2022; Pai et al., 2023; Zheng et al., 2021). For example, Lee et al. prepared a stretchable fiber-shaped strain sensor with high sensitivity and ultra-wide sensing range by synthesizing Ag nanoparticles in multifilament stretchable fibers using hydrazine hydrate (N_2H_4-$4H_2O$) solution to act on absorbed Ag precursors (Lee et al., 2018). However, metal-based fibers are not oxidation-resistant and cannot be degraded, resulting in a short lifespan and generating e-waste that is harmful to the environment. Carbon-based materials, typically carbon black (CB) (Hu et al., 2021), carbon nanotubes (CNTs) (Wang, Sun, et al., 2018), and graphene oxides (GOs) (Wang et al., 2020), exhibit high electrical

---

* Corresponding author.
E-mail address: husanming2022@hbust.edu.cn (S. Hu).

https://doi.org/10.1016/j.carbpol.2024.122963
Received 2 June 2024; Received in revised form 25 October 2024; Accepted 6 November 2024
Available online 14 November 2024

conductivity and excellent mechanical properties and are suitable for constructing flexible strain sensing fibers with large-strain and high sensitivity. For example, Yuan et al. fabricated flexible and stretchable resistive strain sensing fibers by self-assembling CNTs and CB layer by layer on PU fibers (Zhang et al., 2018). The fibers exhibited high sensitivity (gauge factor [GF] up to 45.4), excellent stretchability and good linear detection range (strain range of 15–150 %). The drawback of this type of conductive fiber is that the coated carbon-based conductive layer tends to peel away from the polymer, resulting in weak stabilization as strain sensors. In addition, synthetic polymers used in fibers are nonrenewable and biodegradable. Conductive polymers, such as polypyrrole (PPy) (Wang, Xue, & Zhu, 2019), polyaniline (PANI) (Raman & Ravi Sankar, 2022), and poly(3,4)-ethylenedioxythiophene:poly (styrenesulfonate) (PEDOT:PSS) (Sarabia-Riquelme et al., 2020) have been widely used in the preparation of resistive strain sensing fibers through doping with other polymers or via chemical synthesis. For example, Chen et al. fabricated a PU@PEDOT:PSS composite conductive fiber with core-shell structure using the coaxial microfluidic spinning method (Chen et al., 2024). Fibers with high conductivity (220 S/m) and impressive stretchability (up to and above 400 % strain) as the resistive strain sensor can provide the ultra-sensitive monitoring of human movement. Conductive polymers used to fabricate resistive strain sensing fibers offer advantages in terms of biocompatibility, electrochemical properties, flexibility and ease of chemical modification and synthesis, and good stability. These materials are typically doped or synthesized on other nondegradable synthetic polymers to construct composite conductive fibers (Jo et al., 2022). Hydrogel-based ionic conductive fibers may be used as strain sensors to monitor human movement due to their superior flexibility, softness, stretchability, and recoverable deformability (Hardman et al., 2022; Lu et al., 2024; Wu et al., 2024). For example, Shuai et al. prepared a stretchable (~900 %), conductive (0.69 S/cm), and self-healing PNA/PMA hydrogel fiber, which may be used as a strain sensor for smart fabrics to effectively monitor human body motion (Shuai et al., 2020). However, hydrogel-based ion conductive fibers used as strain sensors for smart fabrics suffer from significant drawbacks in terms of poor spinnability due to poor mechanical strength.

Various conductive fibers can be used as resistive strain sensing fibers for human activity detection. These fibers exhibit outstanding performance in terms of electrical conductivity, tensile properties, detection sensitivity, and flexibility. However, most of these fibers are composed of nonbiodegradable metals and synthesized polymers, which are not environmentally friendly and generate e-waste. In addition, the mechanical strength of fibers prepared by doping/coating with conductive substances or using hydrogel materials remains poor and long-term stability cannot be maintained. Therefore, the design of resistive strain sensing fibers with biodegradability and high mechanical strength has rarely been studied or reported. Notably, many degradable conductive composites have been obtained using cellulose as a substrate (Fatma et al., 2023; Li, Ma, et al., 2022; Wang et al., 2023). Therefore, cellulose, as the most abundant polymer with renewable and biodegradable properties, may serve as a good candidate for the preparation of biodegradable conductive fibers (Liao et al., 2022). Specifically, bacterial cellulose (BC) produced by Acetobacter xylinum (A. xylinum) offers high crystallinity and a three-dimensional network nanofibrous structure (nanofiber with a diameter of 10–100 nm), endowing it with excellent mechanical properties (Wang, Tavakoli, & Tang, 2019). Importantly, the nanostructures and rich —OH groups of BC can provide space and sites for doping or synthesizing conductive materials. Moreover, some studies reported that pure BC macrofibers with high mechanical strength could be prepared by wet stretching and wet twisting methods (Hu, Han, et al., 2022; Wang et al., 2017). Therefore, it may be theoretically feasible to dope or synthesize conductive nanomaterials on BC nanofibers and then prepare conductive macrofibers with high mechanical strength and biodegradability as strain sensors through wet stretching and wet twisting methods. For conductive polymers, although PEDOT has the highest electrical conductivity, its preparation process and cost are higher than those of PPy and PANI. In addition, the conductive stability of PPy is superior to that of PANI, which can be affected by a variety of factors, such as pH, temperature, etc. (Goswami et al., 2023). Therefore, PPy can be selected as a conductive functional material for the preparation of conductive fibers with degradable substrate. Notably, conducting polymer PPy particles may be synthesized in situ through a facile method of oxidizing pyrrole monomers with Fe^{3+}, and their conductivity may be significantly enhanced by doping with P-TSA (Tian et al., 2020). Moreover, many studies have been conducted on the preparation of BC/PPy composite films for supercapacitors (Wang et al., 2016; Xu et al., 2013) interference and electrostatic interference shielding (Huo et al., 2022). As a result, PPy doped with P-TSA (PPy-P) may be used as a functional material to prepare BC/PPy-P composite conductive macrofibers as resistive strain sensors.

In this work, we tested the hypothesis that BC/PPy-P composite conductive macrofibers as resistive strain sensors may effectively monitor mechanical deformation, as well as exhibit high mechanical strength, and be biodegraded without generating e-waste. Through the in-situ polymerization of PPy-P particles on BC nanofibers, BC/PPy-P composite conductive macrofibers were prepared by wet-stretching and wet-twisting methods. The physicochemical properties of the fabricated BC/PPy-P composite macrofibers were systematically characterized in terms of their morphology, chemical structures, electrical conductivity, electrothermal properties, and mechanical strength. In addition, the biodegradability of the BC/PPy-P composite macrofibers was characterized, and the performance of BC/PPy-P conductive macrofibers as resistive strain sensors were investigated. For practical applications, we tested macrofibers sewn into fabrics for the monitoring of human movement.

2. Experimental section

2.1. Chemicals and materials

BC hydrogels (purity of 99.4 %, crystallinity ~85 %, molecular weight ~3.25×10^5 kDa, nanofiber diameter of 20–100 nm) with a thickness of 4 mm after water absorption were purchased from Hainan Guangyu Biotechnology Co., Ltd. (China). Cellulase (enzyme activity of 400 U/g) was purchased from Dongheng Huadao Biotechnology Ltd. (China). Pyrrole, sodium hydroxide sodium acetate, ferric chloride hexahydrate ($FeCl_3{\cdot}6H_2O$), and anthrone, p-toluenesulfonic acid (P-TSA) were purchased from Shanghai Macklin Biochemical Technology Co., Ltd. and used as received. Concentrated sulfuric acidchloroform, n-butanol, potassium sodium tartrate, acetic acid, and recrystallized phenol were purchased from Shanghai Sinopharm Chemical Reagent Co., Ltd. and used without further purification.

2.2. Preparation of the BC/PPy-P conductive macrofibers

First, the purchased BC was cut into long strips with a width of 6 mm and soaked in distilled water to fully absorb the water for purification (Fig. S1a and b). The swollen BC strips were then mechanically compressed using a compressor (100 N pressure) for 1 min to remove some of the absorbed water (Fig. S1c). Subsequently, the compressed BC strips were immersed in a solution of Fe^{3+} and shaken in a shaker (150 rpm) for 1 h and Fe^{3+} was allowed to fully diffuse in the three-dimensional network structure of BC to obtain BC/Fe^{3+} composite strips (Fig. S1d and e). Next, BC strips with absorbed Fe^{3+} were placed into Py/P-TAS mixed solution for the in situ polymerization reaction to form the PPy-P particles (Fig. S1f). The temperature and time of the reaction were controlled at 4 °C and 1 h, respectively. Subsequently, the prepared 10 BC/PPy-P composite strips (Fig. S1g) were immersed in 1 L of distilled water and washed repeatedly to remove any excess chemicals and impurities. The water was changed every 12 h for 4 days until the distilled water was colorless. Subsequently, the BC/PPy-P composite strip was elongated by 20 % via wet-drawing to achieve better orientation of the nanofibers (Fig. S1h). Finally, BC/PPy-P composite conductive macrofiber was obtained by wet-twisting the composite strip to 95 % of its original length and drying at room temperature in a tensile state with a loading of 100 g (Fig. S1i). As a control, BC macrofibers were also obtained by wet-drawing and wet-twisting methods. The molar ratio of Fe^{3+}, Py monomer, and P-TSA was 2.6:1:1. The Fe^{3+} solutions were established with 5 concentrations of 0.05, 0.1, 0.2, 0.3, 0.4 and 0.5 mol/L, and the prepared conductive composite fibers were abbreviated as BC/PPy-P1, BC/PPy-P2, BC/PPy-P3, BC/PPy-P4, and BC/PPy-P5, respectively. In addition, to investigate the effect of P-TSA on the electrical conductivity of composite macrofibers in this work, BC/PPy macrofibers were prepared using the same method without the addition of P-TSA. Unless otherwise specified, BC/PPy-P macrofibers in this work refer to BC/PPy-P4 macrofibers.

2.3. Biodegradation of the BC/PPy-P macrofibers

First, 150 mL of 0.2 mol/L sodium acetate mother liquor was mixed with 100 mL of 0.2 mol/L acetic acid mother liquor, and the mixed solution was diluted to 1 L with distilled water to obtain the acetic acid buffer solution with a pH of 4.8. Then, 0.5 g of cellulase was added to 100 mL of acetate buffer to obtain the degradation solution. Next, BC fibers and BC/PPy-P fibers were separately added to the degradation solution and degraded in a water bath at 50 °C. Subsequently, 2 mL of degradation solution was obtained every 12 h for total sugar content testing, and photographs were taken to observe the state of the macrofibers. Multiple sets of experiments were conducted to weigh the mass of the dried fibers every 12 h to observe the change in weight during fiber degradation.

2.4. Characterization

The morphologies and microstructures of all samples were obtained by using an S-4800 field emission scanning electron microscope (FE-SEM) after gold sputtering for 240 s. The distribution of major elements in the BC/PPy-P macrofiber cross sections was also captured by utilizing the FE-SEM machine. The X-ray photoelectron spectroscopy (XPS) patterns of the BC/PPy-P macrofibers were recorded by an X-ray photoelectron spectrometer (AXIS-ULTRADLD-600W). The X-ray diffraction (XRD) spectra were acquired by an XRD spectrometer (XRD-7000, MAXima.X) in the scanning range of 5°–70° with a scanning speed of 10°/min. The Fourier transform infrared (FTIR) spectra of samples were measured by a VERTEX 70 spectrometer in the spectral range of 400–4000 cm^{-1}. A thermal analyzer (Pyris1 TGA) was employed to analyze the thermal stability of samples ranging from 30 °C to 800 °C at a heating rate of 10 °C/min under a nitrogen atmosphere. The mechanical properties of the BC, BC/PPy, and BC/PPy-P macrofibers were characterized by a universal testing machine (UTM6503, SUNS Industrial Testing System Co., Ltd., China). All sensing properties of the BC/

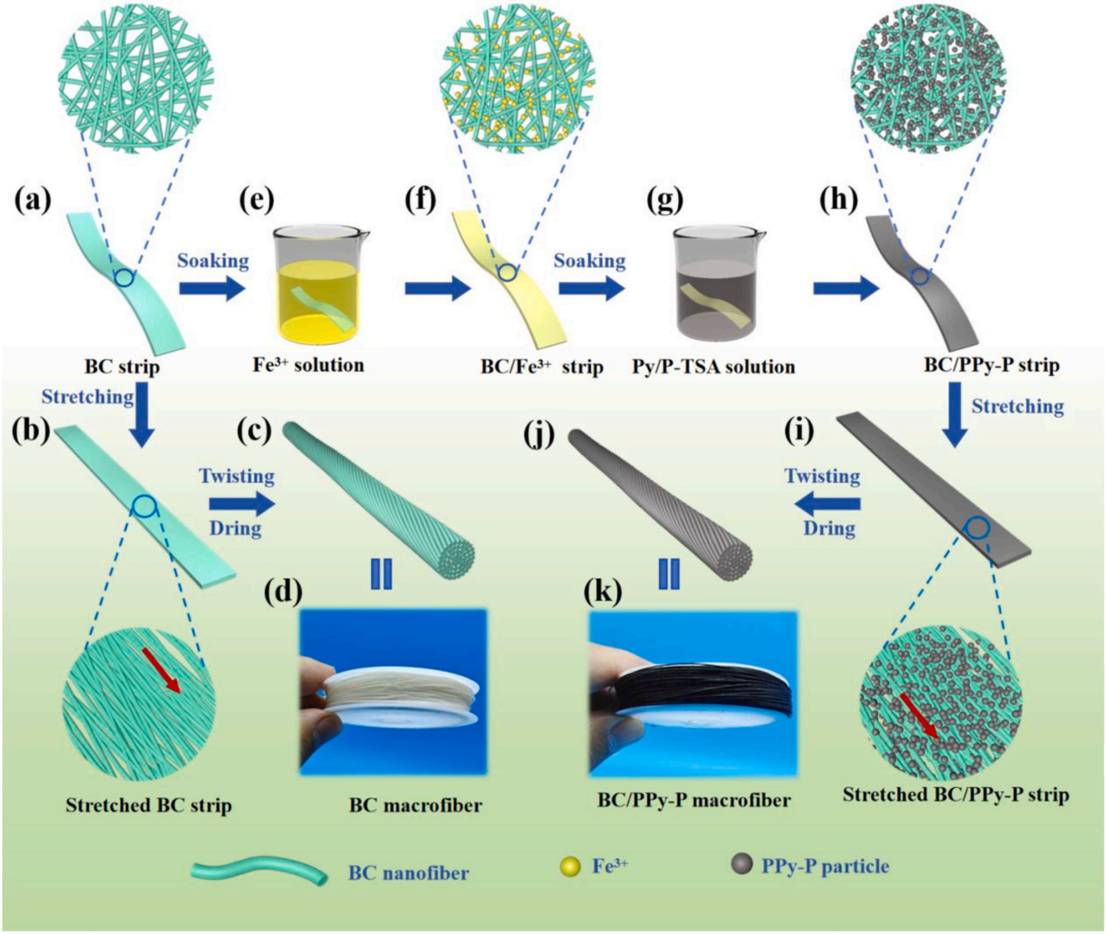

Fig. 1. Schematic diagram showing BC and BC/PPy-P macrofiber preparation: (a) BC strip; (b) stretched BC strip; (c) BC macrofibers obtained by twisting the stretched BC stripe and drying; (d) optical photographs of the BC macrofibers; (e) BC strip immersed in Fe^{3+} solution, and then shaking for 1 h to allow for the full absorption of Fe^{3+} to obtain the BC/Fe^{3+} strip (f); (g) immersion of the BC/Fe^{3+} strip into Py/P-TSA solution to undergo in situ polymerization to form PPy-P; (h) BC/PPy-P composite strip; (i) stretched BC/PPy-P strip; (j) obtained BC/PPy-P macrofiber by twisting the stretched BC/PPy-P strip and drying; (d) optical photographs of the BC/PPy-P macrofibers.

PPy-P macrofibers were assessed by a high-precision multimeter (DMM7510), and polyimide (PI) films were used to support the bending deformation of the macrofibers. The regular bending behavior of the macrofibers during the test was accomplished by a mechanical stretching apparatus. Moreover, the conductive BC/PPy-P macrofibers were sewn into gloves, pants, and a top to monitor body movement.

3. Results and discussion

3.1. Preparation and morphological characterization of the BC/PPy-P macrofibers

Fig. 1 shows the schematic preparation process and actual morphology of the pure BC and BC/PPy-P macrofibers. Meanwhile, Fig. S1 shows the digital images of the BC/PPy-P macrofibre preparation process. Initially, pure BC film was cut into long strips with a width of 6 mm for later use (Fig. 1a). Pure BC macrofiber was then fabricated directly by wet-stretching and wet-twisting of the BC strips (Fig. 1b and c). The purpose of stretching BC was to endow the nanofibers with better orientation, which effectively increased the mechanical strength of the macrofibers (Wang et al., 2017). The stretched BC was wet-twisted and then dried under a stretched state (loading with 100 g) at a temperature of 30 °C in the oven for 2 h to obtain the BC macrofibers (Fig. 1d). The BC/PPy-P composite conductive macrofibers were fabricated by wet-stretching and wet-twisting of the BC/PPy-P complexes. The complexes were synthesized through the in situ synthesis of PPy doped with

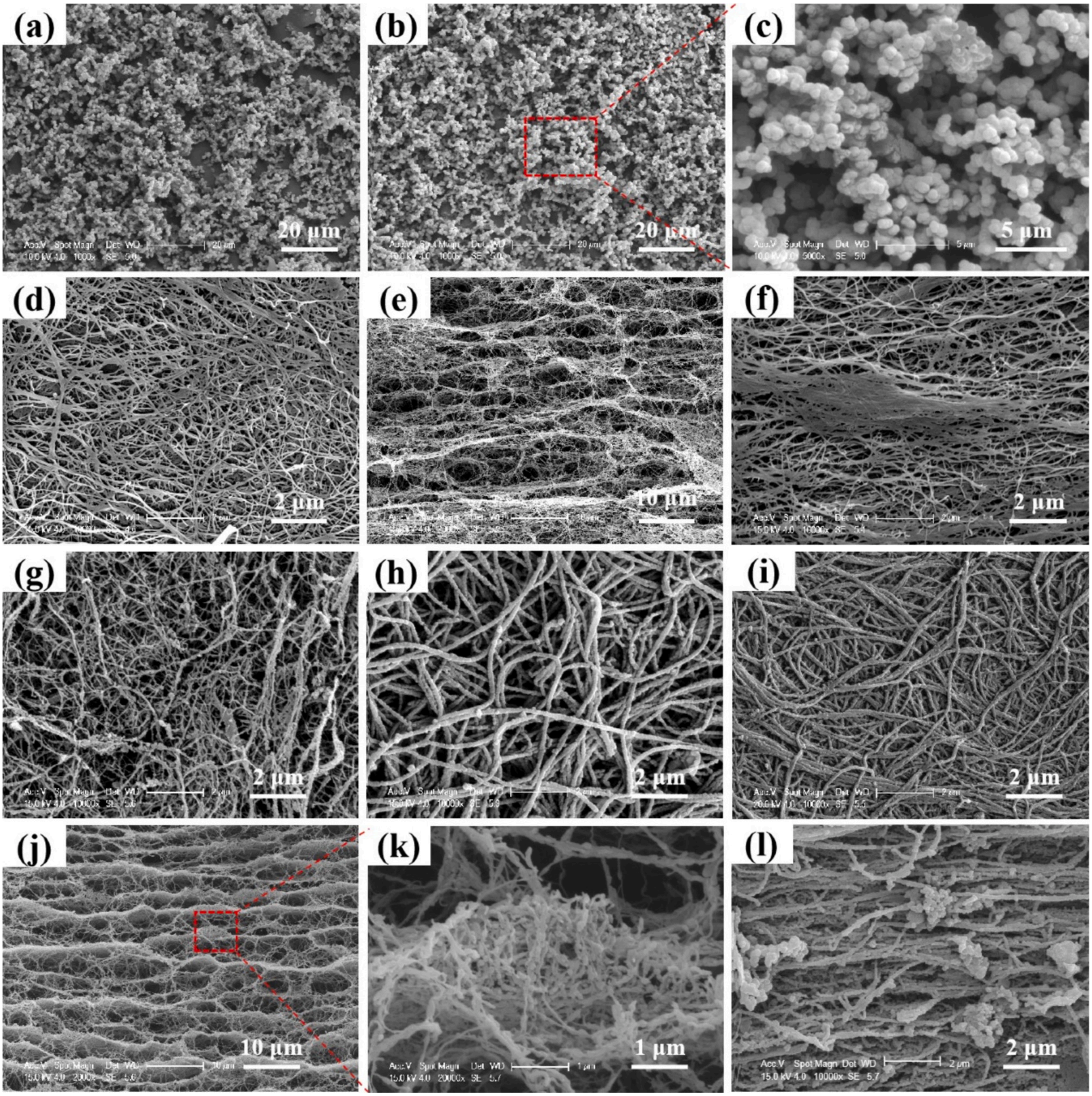

Fig. 2. SEM images of the PPy and PPy-P particles, as well as the BC, BC/PPy, and BC/PPy-P membranes: (a) PPy particles; (b, c) PPy-P4 particles; (d) surface morphology and (e) cross-sectional morphology of the BC membrane; (e) surface morphology of the stretched BC membrane; surface morphologies of the (g) BC/PPy-P1, (h) BC/PPy-4, and (i) BC/PPy-P4 membranes; (j, k) cross-sectional morphologies of the BC/PPy-P4 membrane; (l) surface morphology of the stretched BC/PPy-P4 membrane.

P-TSA in the 3D nano-network structure of BC. The BC strips were first immersed in Fe^{3+} solution and shaken in a shaker (150 rdm) for 1 h, which allowed the Fe^{3+} ions to fully diffuse into the network structure of BC to obtain the BC/Fe^{3+} complexes (Fig. 1e and f). Then, the BC complexes were immersed in a mixed solution of pyrrole and P-TSA, and left at 4 °C for 1 h to prepare the BC/PPy-P composite strips, as shown in Fig. 1g and h. During the process, the oxidant Fe^{3+} ions made contact with the pyrrole monomers and P-TSA molecules, causing the pyrrole monomers to undergo a polymerization reaction and produce PPy-P particles in the network structure of BC. The reaction process is shown in Fig. S2. The introduction of P-TSA as a dopant significantly improved the electrical conductivity of PPy (Tian et al., 2020). Finally, as demonstrated by the pure BC macrofibers, the BC/PPy-P composite conductive macrofibers were fabricated by the wet-stretching and wet-twisting of the BC/PPy-P composite strips (Fig. 1i and j). A more detailed preparation process is provided in Section 2.2. Comparison of Fig. 1d and k indicated that the BC/PPy-P composite conductive macrofibers were transformed from white pure BC macrofibers to black fibers due to the presence of PPy-P particles.

Fig. 2a and b show the SEM images of the PPy particles (undoped P-TSA) and PPy-P particles. No significant difference was observed in the size of the two types of particles. Additionally, sticky phenomena occurred between both types of particles, as clearly shown in Fig. 2c. The sticky phenomenon facilitated the encapsulation of BC nanofibers by the

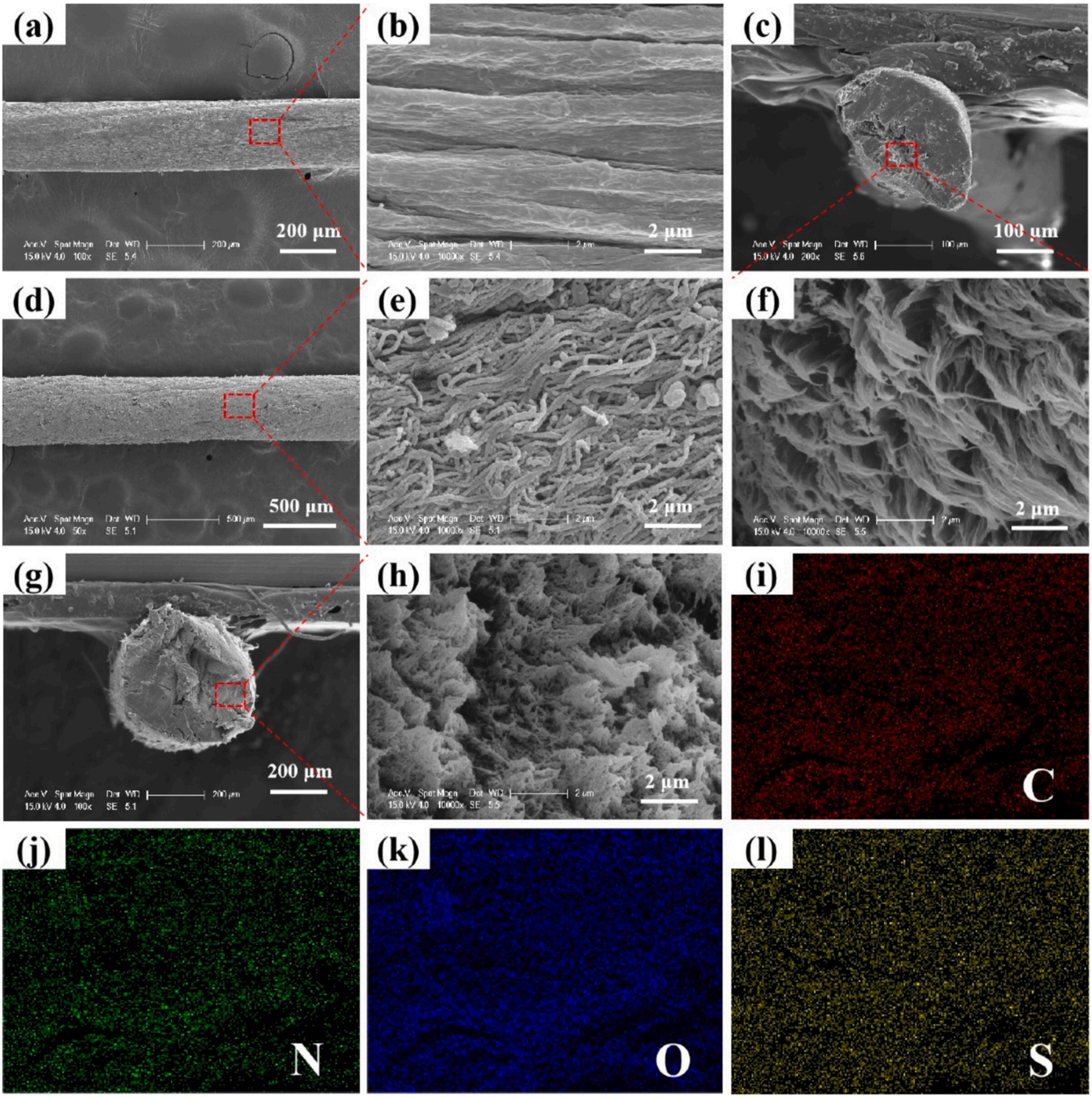

Fig. 3. SEM images of BC and BC/PPy-P macrofibers, analysis of the elemental distribution of BC/PPy-P macrofibers in the cross-sectional SEM images; (a, b) surface morphology and (c, f) cross section of the BC macrofibers; (d, e) surface morphology and (g, h) cross section of the BC/PPy-P macrofibers; (i-l) elemental distribution of C, N, O, and S in the BC/PPy-P macrofibers.

PPy-P particles. This was possibly conducive to the transfer of electrons, which improved the electrical conductivity of the BC/PPy-P macrofibers. Fig. S3 shows the SEM images of the PPy-P particles and the corresponding mapping of C, N, O, and S elements. The uniform distribution of N and S elements tentatively indicated the successful synthesis of PPy doped with P-TSA. Fig. 2d and e show the microstructure of the BC membrane surface and cross section. BC exhibited a three-dimensional nano-network structure and the cross section demonstrated an obvious hierarchical structure. Fig. 2f shows the SEM image of the BC surface after 30 % stretching. The stretched BC exhibited a better nanofiber orientation than the unstretched BC in Fig. 2d. Fig. 2g and h show the surface SEM images of the BC/PPy-P1 and BC/PPy-P4 composite membranes, respectively. The nanofibers of BC were encapsulated by the PPy-P particles, resulting in an increase in nanofiber diameter compared to pure BC. Moreover, the nanofiber diameter of the BC/PPy-P4 composite strip was significantly larger than that of BC/PPy-P1, indicating that more PPy-P particles were wrapped on the surface of the BC nanofibers of the BC/PPy-P4 composite membrane, resulting in better obtained electrical conductivity. Therefore, this tentatively suggested that the electrical conductivity of the BC/PPy-P composite materials could be modulated by controlling the concentration of raw materials during the preparation process. Fig. 2i presents the SEM image of the BC/PPy-4 composite strip surface. The BC/PPy-4 composite strips had smaller nanofiber diameters than BC/PPy-P4, indicating that the BC/PPy-P4 macrofibers contained more PPy-P. This could be verified by the elemental analysis results of the samples. As shown in Table S1, the BC/PPy-P4 macrofibers contained 25.18 % PPy-P, while the BC/PPy-4 macrofibers contained only 0.22 % PPy-P. Therefore, the doping of P-TSA was possibly beneficial to improving the conductivity of the BC/PPy-P macrofibers. The cross-sectional micro-layered structure of the BC/PPy-P4 composite strip is shown in Fig. 2j. Fig. 2k presents a partial enlargement of Fig. 2j, which indicated that the PPy-P particles were also fully wrapped with the BC nanofibers. Similarly, the nanofibers of the stretched BC/PPy-P composite strips demonstrated good orientation along the stretching direction (Fig. 2l). Good nanofiber orientation of BC/PPy-P composite strips not only improved the mechanical strength of the prepared microfibers, but also increased the electrical conductivity.

Fig. 3a and b present the SEM images of the pure BC macrofiber surface. The wet-drawing and wet-twisting preparation methods, combined with a slow drying process in the stretched state, resulted in BC macrofibers with a dense nanofiber structure due to the formation of hydrogen bonds between the nanofibers (Wang et al., 2017), as shown in the cross-sectional SEM images of the BC microfibers (Fig. 3c and f). Fig. 3d and e show the surface of the BC/PPy-P macrofiber and its localized magnified SEM images. The BC/PPy-P macrofiber had a rougher and looser surface structure than the pure BC macrofiber due to the presence of PPy-P isolating the BC nanofibers. As shown in Fig. 3e, the nanofibers encapsulated by PPy-P were well oriented, which facilitated the procurement of macrofibers with superior electrical conductivity and mechanical strength. Additionally, the BC/PPy-P macrofibers had a dense cross-sectional structure, and larger diameter than the pure BC macrofibers (Fig. 3g and h). Fig. 3i–l show the mapping distribution of the four elements (C, N, O, and S) and the energy-dispersive spectrum in the cross section of the BC/PPy-P macrofibers. The energy spectra of the corresponding elements are shown in Fig. S4. The presence of S elements was due to the introduction of P-TSA and the N elements were derived from the pyrrole ring. The uniform distribution of S elements indicated that P-TSA was successfully grafted onto PPy. Significantly, the conductivity of PPy doped with P-TSA could be substantially increased up to 200 S/cm from 10^{-6} S/cm of undoped PPy (Li et al., 2006). More importantly, the elemental distribution diagrams demonstrated that PPy-P had a uniform distribution in the BC network structure, which effectively ensured that the BC/PPy-P macrofibers achieved good electrical conductivity.

3.2. XRD and FTIR spectroscopy

Several chemical structure characterization methods were used to demonstrate the successful synthesis of PPy-P in the BC network. The crystal structure and integration of PPy-P and BC was confirmed by the XRD patterns, as shown in Fig. 4a. First, the characteristic peaks of PPy and PPy-P consisted of broad reflection peaks with an obvious amorphous state. Additionally, BC, BC/PPy, and BC/PPy-P exhibited consistent characteristic peaks at $2\theta = 14.6^\circ$, 16.8°, and 22.5°, only with reduced intensity, which corresponded to the (110), (101), and (202) reflections of type I cellulose planes, respectively (Hu, Zheng, et al., 2022). This indicated that the in-situ polymerization of PPy and the doping of P-TSA did not change the crystal structure of BC, but only reduced the crystal content. Fig. 4b shows the FTIR spectra of BC, PPy, PPy-P, BC/PPy, and BC/PPy-P, where the specific chemical functional groups could be characterized. The characteristic peaks of BC appeared at 3342, 2895, 1160, and 1060 cm^{-1}, corresponding to the stretching vibrations of —OH, C—H, C—O, and C—O—C, respectively (Hu, Han, et al., 2022), and the typical absorbance peaks of absorbed water at 1644 cm^{-1} represented O—H bending. The characteristic peaks of PPy shown in the regions of 1447, 1297, 1040, and 835 cm^{-1} corresponded to C—C, C—N stretching of aromatic amine, ═C—H bending, and N—H wagging of the out of plane PPy ring (Peng et al., 2016), respectively. The peak at 1537 cm^{-1} was attributed to the C═C vibrations in the aromatic ring of pyrrole. The peak at 778 cm^{-1} corresponded to the ═C—H bond, which represented the bending deformation vibration of the pyrrole ring and the substitution vibrations of the benzene ring in the PPy-P particles. This indicated that PPy-P was successfully synthesized inside BC. Additionally, the characteristic peak of the sulfonic acid group appeared in the region of 1038 cm^{-1}, which indicated that P-TSA was present with a doped state inside the BC/PPy-P substance. Many characteristic peaks of BC and PPy-P were observed in the BC/PPy-P composite macrofibers, demonstrating that a satisfactory chemical structure was achieved. In addition, BC/PPy-P demonstrated characteristic peaks that showed significant shifts, such as the N—H and sulfonic acid groups (—HSO_3). This was possibly due to the formation of hydrogen bonds between the O—H of BC, the N—H of pyrrole, and the —HSO_3 of P-TSA. However, the hydrogen bonds possibly served as a traction force to assist the PPy warped BC nanofibers and avoid the large-scale aggregate formation of the PPy-P particles.

3.3. XPS analysis

In addition, the XPS wide-scan spectra of the BC/PPy-P fiber and its raw materials, as well as the high-resolution spectra of N 1s and S 2p, are shown in Fig. 4c–f. The ratio of C to O in the BC-based composite fibers gradually increased with the synthesis of PPy and the doping of P-TSA (Fig. 4c). Additionally, the peak of N 1s at 400 eV appeared in the BC/PPy and BC/PPy-P composite macrofibers. These results provided a preliminary indication of the successful synthesis of PPy in BC. As shown in Fig. 4d and e, the N 1s spectra verified that the N—H (peak at 399.3) and C—N (peak at 400.4) groups were both present in the BC/PPy and BC/PPy-P composite macrofibers. N—H and N—C were derived from the pyrrole ring, demonstrating the successful synthesis of PPy. After doping with P-TSA, the characteristic peaks produced a small shift for the BC/PPy-P composite macrofibers, which was attributed to intermolecular interactions between PPy and P-TSA. The characteristic peak of PPy-P at 405 eV for N-S appeared in BC/PPy-P, as shown in Fig. 4e. Moreover, the S 2p spectra of BC/PPy-P could be decomposed into two peaks at 167.5 and 169.5 eV, which belonged to the binding energies of S 2p1/2 and S 2p3/2 of the —HSO_3 group of P-TSA, respectively (Thombal & Han, 2018). These results provided that PPy doped with P-TSA was successfully synthesized in the BC/PPy-P composite macrofibers.

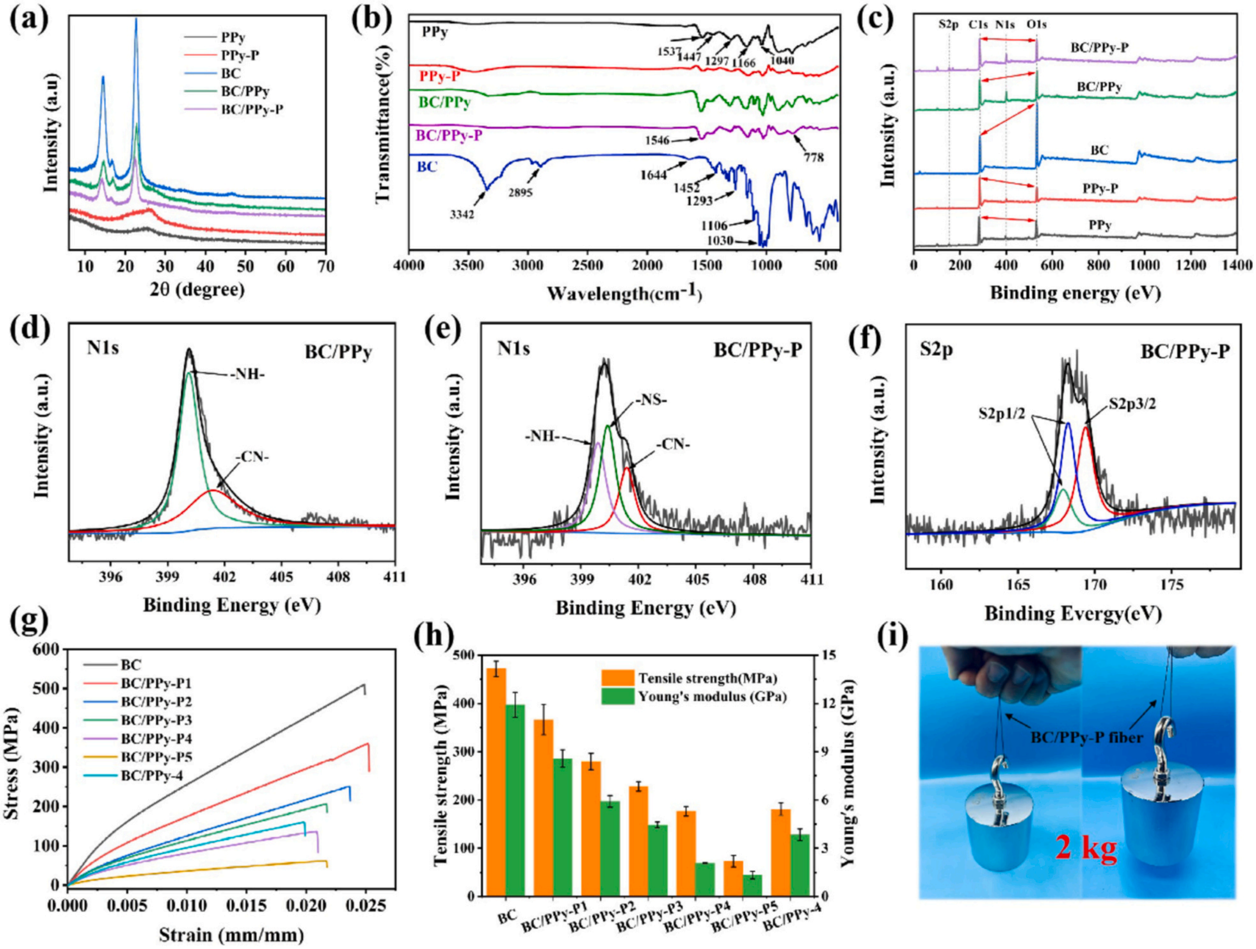

Fig. 4. Chemical structure and mechanical property characterization of the macrofibers: (a) XRD patterns, (b) FTIR spectra, and (c) XPS survey spectrum of PPy, PPy-P, BC, BC/PPy, BC/PPy-P; high-resolution N 1s XPS spectra of (d) BC/PPy macrofiber and (e) the BC/PPy-P macrofibers; (f) high-resolution S 2p XPS spectra of the BC/PPy-P macrofibers; (g) stress–strain curves, and (h) tensile strength and Young's modulus of the BC, BC/PPy, and BC/PPy-P macrofibers; (i) BC/PPy-P macrofibers lifting a 2-kg weight.

3.4. *Mechanical property analysis*

The mechanical properties of the BC/PPy-P composite conductive macrofibers were characterized and the effects of PPy and P-TSA on the mechanical properties of macrofibers were investigated. Fig. 4g and h display the strain–stress curves and corresponding tensile strength and Young's modulus of the pure BC, BC/PPy-4, and BC/PPy-P macrofibers. The pure BC macrofibers had the highest mechanical strength, as shown in Fig. 4g. This was attributed to the fact that the pure BC macrofiber had the densest nanofiber structure, which was evident from the SEM images of the macrofiber surface (Fig. 3b) and because the BC macrofibers possessed the smallest diameter among all types of macrofibers (Table S1). This dense nanofiber structure was attributed to strong hydrogen bonding between the BC molecules. For the BC/PPy-P composite macrofibers, hydrogen bonding interactions between the BC molecules were weakened with the introduction of PPy, and the surface roughness of the BC nanofibers wrapped by PPy significantly increased, leading to a looser nanofiber structure. Therefore, compared to the pure BC macrofibers, the mechanical strength of the BC/PPy-P composite macrofibers significantly decreased. For different BC/PPy-P macrofibers, the mechanical strength decreased with increasing concentration of the reactive raw material solution. This was due to the fact that a higher concentration of reactants produced more PPy-P wrapped around the nanofibers of BC, which produced a looser fiber structure of the BC/PPy-P fibers, resulting in a decrease in mechanical strength. As shown in Table S1, the diameter of the BC/PPy-P macrofibers and the PPy-P content gradually increased with an increase in pyrrole concentration. Additionally, previous SEM images demonstrated that the nanofiber diameter in the BC/PPy-P4 macrofibers was larger than that of BC/PPy-P1 due to the encapsulation of more PPy-P agglomerated particles (Fig. 2g and h). The mechanical strength of the BC/PPy macrofibers without P-TSA doping was slightly stronger than that of the BC/PPy-P macrofibers. This was possibly due to the fact that the amount of synthesized PPy was less than that of PPy-P, as indicated in the microscopic SEM images (Fig. 2h and i) and in Table S1. Overall, the tensile strength and Young's modulus of the BC/PPy-P macrofibers were inferior to the pure BC macrofibers, as shown in Fig. 4h. Both the tensile strength and Young's modulus of the BC/PPy-P macrofiber decreased with increasing reactant concentration. The elastic strength and Young's modulus decreased from 366 MPa and 8.4 GPa for the BC/PPy-P1 macrofibers to 76 MPa and 1.4 GPa for the BC/PPy-P5 macrofibers, respectively. This was mainly due to the increase in PPy-P content and the structure becoming looser, as well as the brittle nature of PPy-P (Tian et al., 2020). Due to the high degree of orientation and dense arrangement of nanofibers, the BC macrofibers served as a basic framework that supported the entire structure of the BC/PPy-P fibers. Although the mechanical properties of the BC/PPy-P macrofibers were relatively weakened, benefiting from the high mechanical strength of the BC macrofibers, the mechanical properties of the BC/PPy-P4 (~177 MPa of tensile strength and ~1.6 GPa of Young's modulus) macrofibers was well maintained, and these fibers could lift a 2-kg weight without breaking (Fig. 4i).

3.5. TGA and electrothermal property analysis

In addition to the mechanical properties, the thermal stability of the BC/PPy-P composite conductive macrofibers is considered crucial for different environments. The thermal properties of the BC macrofibers, PPy-P particles, BC/PPy-P1, and BC/PPy-P4 macrofibers were characterized, as shown in Fig. 5a. The residual quality of BC and PPy-P at 800 °C was maintained at 3.5 % and 57.4 %, respectively. For the BC/PPy-P composite macrofibers, the BC/PPy-P1 composite macrofibers degraded at 340 °C and the last mass was maintained at 5.8 %, while the BC/PPy-P4 composite macrofibers degraded at 290 °C and the final mass was maintained at 38.7 %. Clearly, PPy-P endowed the BC/PPy-P composite conductive fibers with good thermal stability. The electrothermal effect of the BC/PPy-P composite conductive macrofibers was also studied. As shown in Fig. 5b and c, the macrofibers were tested under different voltages by utilizing the polyimide film as the substrate. Pictures taken by a thermal imaging camera showed that the temperature of the macrofibers increased as the applied voltage increased (Fig. 5c_1–c_6). In addition, the temperature increased from 19.8 °C to 75.5 °C as the voltage increased from 3 to 17 V (Fig. 5d). The BC/PPy-P composite conductive macrofibers also possessed fast thermal response (~15 s) to different temperatures when different voltages were applied (Fig. 5e).

3.6. Electrical conductivity analysis

Electrical conductivity is considered one of the most important properties of macrofibers that reflects application potential. As shown in Fig. 5f, pure BC macrofibers exhibited high electrical insulation properties with resistance reaching 5×10^4 MΩ. After the in situ polymerization of PPy and doping of P-TSA, the conductivity of the BC/PPy-P macrofibers was significantly improved. This was because the layer of PPy-P particles wrapped around the outside of the BC nanofibers constructed a conductive pathway for external electron transfer. As is shown in Fig. S5, the effect of the concentration of the reactants on the electrical conductivity of the PPy-P particles was not significant. However, the concentration of reactants had a great influence on the electrical conductivity of the prepared BC/PPy-P macrofibers. More specifically, a higher concentration of reactants led to a higher content of synthesized PPy-P (Table S1, Supporting Information), resulting in a higher electrical conductivity of the prepared BC/PPy-P macrofibers. The electrical conductivity increased from 0.0015 S/cm for BC/PPy-P1 macrofiber (PPy-P content of 9.7 %) to 7.19 S/cm for the BC/PPy-P5 macrofiber (PPy-P content of 66.1 %). Notably, the electrical conductivity values of the BC/PPy-4 and BC/PPy-P4 macrofibers were 0.09 and 5.33, respectively, which relatively increased by nearly 60 times after doping, indicating that the doping of P-TSA could significantly improve the electrical conductivity of the BC/PPy macrofibers. From the image of Fig. S5, doping of p-TSA greatly enhances the electrical conductivity of PPy (from ~0.3 S/cm for PPy particles to ~42 S/cm for PPy-P particles). As shown in the inset of Fig. 5f, the BC/PPy-P4 macrofibers could light up an LED under a state of applied voltage. Therefore, combining these mechanical properties, the BC/PPy-P4 fibers demonstrated the most integrated performance, which could be used to design specific applications.

3.7. Degradability of the BC/PPy-P macrofibers

Previous results showed that BC hydrogels could be degraded by cellulase in 6 h (Zhang et al., 2021). The process and principle of BC nanofiber degradation by cellulase were mentioned in our previous study (Hu, Han, et al., 2022). However, remains unclear whether BC nanofibers encapsulated by PPy-P particles can be successfully degraded in cellulase solution. Therefore, the state of BC/PPy-P composite conductive macrofibers and pure BC macrofibers in cellulase solution was consecutively recorded, as shown in Fig. 6a and b. It was clear that BC macrofibers were degraded in the cellulase solution within 60 h, while BC/PPy-P macrofibers were degraded after 132 h, leaving only black BC/PPy-P particles. As a result, the degradation of nanofibers in the BC/PPy-P macrofibers was slower than in the BC macrofibers, due to

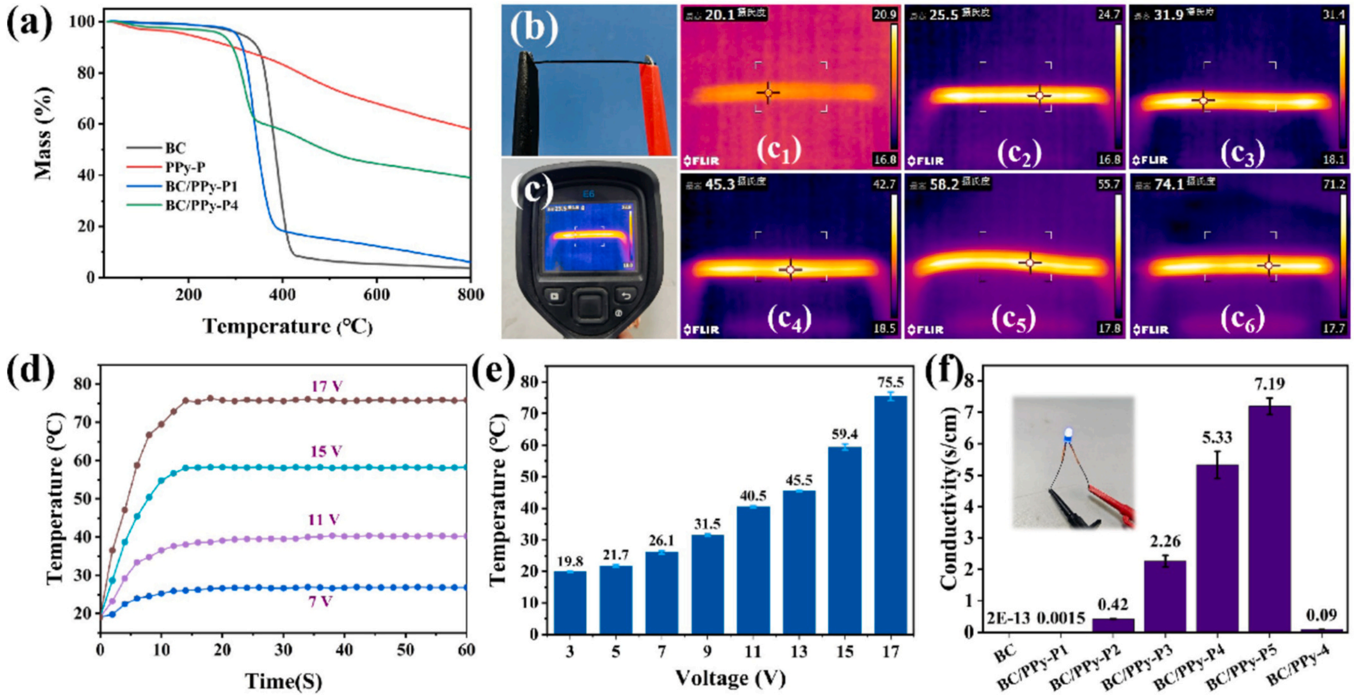

Fig. 5. Thermal and electrical properties of the BC/PPy-P macrofibers: (a) TGA curves of the BC macrofibers, PPy-P particles, BC/PPy-P1, and BC/PPy-P1 macrofibers; (b, c) digital image of the BC/PPy-P macrofibers when switched on at different voltages; (c_1-c_6) temperature diagrams of the BC/PPy-P macrofibers at different voltages; (d) time−temperature curve of the BC/PPy-P macrofibers; (e) temperature and voltage diagram of the BC/PPy-P macrofibers; (f) electrical conductivity of the BC/PPy-P macrofibers (inset, BC/PPy-P macrofiber as a conductor lights up the LED when connected to the power supply).

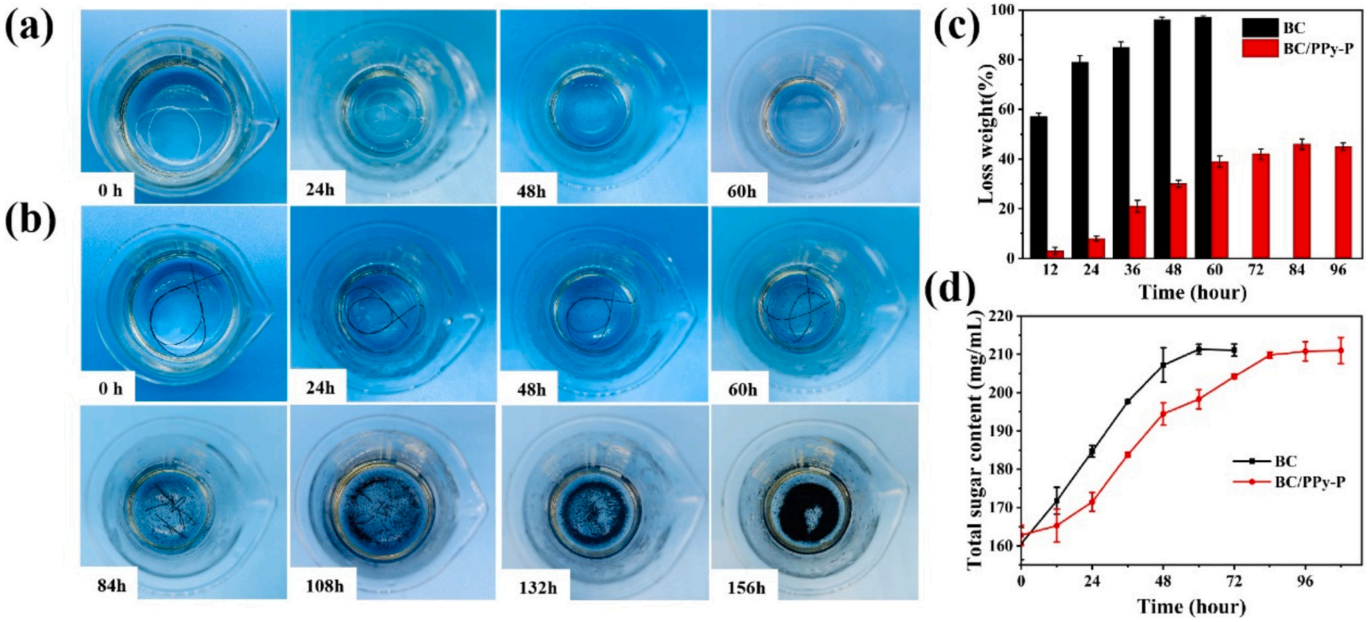

Fig. 6. Degradation properties of the BC/PPy-P microfibers in the cellulase solution: digital image of (a) the BC microfibers and (b) BC/PPy-P macrofibers during degradation; (c) total sugar content in the cellulase solution and (d) loss weight of the BC and BC/PPy-P macrofibers during degradation.

the encapsulation of PPy-P hindering the contact of BC nanofibers with the cellulase solution. To more accurately determine the degradation time and degradation rate changes of the BC/PPy-P macrofibers, the loss mass of the BC and BC/PPy-P macrofibers during degradation was calculated (Fig. 6a). In addition, their total sugar content in the degradation solution was measured (Fig. 6d). As shown in Fig. 6c, pure BC macrofibers lost about 57 % of their weight in the first 12 h of the degradation process, while the BC/PPy-P macrofibers lost only 3 % of their weight. As shown in Table S1, the BC content in the BC/PPy-P macrofibers was about 44 % (~56 % of PPy-P particles). Thus, the loss of BC in the BC/PPy-P macrofibers in the first 12 h was 6.8 %, which was significantly less than 57 %. This result also indicated that the degradation rate of BC in the BC/PPy-P macrofibers was slower than that of the BC macrofibers. After 48 h of degradation, the weight loss of BC was about 97 %, while after 84 h of degradation, the weight loss of BC/PPy-P fibers was about 43 %, with no significant change in their weight loss as degradation proceeded. These results illustrated that pure BC and BC/PPy-P macrofibers could be completely degraded within 48 h and 84 h, respectively. Furthermore, the change in total sugar content in the solution also reflected the characteristics of macrofiber degradation. As shown in Fig. 6d, the total sugar content in the degradation solution of the BC and BC/PPy-P macrofibers did not increase after 48 h and 84 h, respectively. In addition, the total sugar content in the degradation solution of the BC macrofibers was higher than that of the BC/PPy-P macrofibers, and was approximately equal after complete degradation. In summary, the BC/PPy-P macrofibers could be completely degraded by cellulose within 84 h, leaving only biocompatible PPy-P particles, which could be recycled for other uses. Biodegradability of the BC/PPy-P conductive macrofiber demonstrated their potential for the preparation of environmentally friendly and green wearable electronic devices.

3.8. Performance analysis of BC/PPy-P macrofibers as resistive strain sensors

Benefiting from excellent biodegradability, electrical conductivity, and mechanical strength, the BC/PPy-P macrofiber showed potential for wearable smart fabrics. The performance and applications of the BC/PPy-P macrofibers as fiber-shaped resistive strain sensors were explored. To achieve more accurate and sensitive detection of resistance changes under deformation, PI films were used to support the BC/PPy-P macrofiber, as shown in the inset of Fig. 7a, where $(R - R_0)/R_0$ was used to represent the relative resistance changes during macrofiber bending, with R_0 the initial resistance of the macrofiber without bending, R the resistance during bending. When the BC/PPy-P conductive macrofiber was bent under force, one side of the PPy-P was stretched and the other side of the PPy-P was compressed, resulting in an inhomogeneous structure of the macrofiber conductive pathway, which was not conducive to electron transport and led to an increase in resistance. When the external force was removed, the structure would recover and the resistance would return to its initial value. Thus, BC/PPy-P conductive macrofibers could realize excellent sensing properties with a small volume. As shown in Fig. 7a, the BC/PPy-P macrofibers exhibited nearly uniform relative resistance changes when subjected to continuous 20° bending deformation. Fig. 7b illustrates the amplified waveform of the relative resistance change produced by a single deformation. The response and recovery times for detection were 67 and 95 ms, respectively, demonstrating that the BC/PPy-P macrofibers possessed sensitive sensing of bending deformation. Additionally, the sensing performance of the BC/PPy-P macrofibers to different degrees of bending at the same frequency was investigated, as shown in Fig. 7c. The relative resistance changes of the BC/PPy-P macrofibers increased with increased bending angle (increasing from 4.3 at 20° to 17.2 at 80°), demonstrating it had a wide detection range. Furthermore, the sensitivity of the BC/PPy-P macrofibers as resistive strain sensors was calculated (Fig. 7d). The sensitivity was 0.23 at the stage of 5–30°, which transformed to 0.19 at 40–80°. The sensitively was defined as the ratio of $\Delta((R - R_0)/R_0)$ and ΔA, where R is the resistance value of the macrofiber during bending, R0 is the initial value of the sensor without bending, and A is the angle of bending. In addition, a long service life of the sensor was important to ensure economic practicality. The BC/PPy-P macrofiber was subjected to repeated bending cycles, as shown in Fig. 7e and f. The BC/PPy-P macrofiber possessed an expected service life, allowing it to be reused more than a thousand times without signal degradation. The results showed that the BC/PPy-P macrofiber possessed durable and stable sensing performance as a resistive strain sensor.

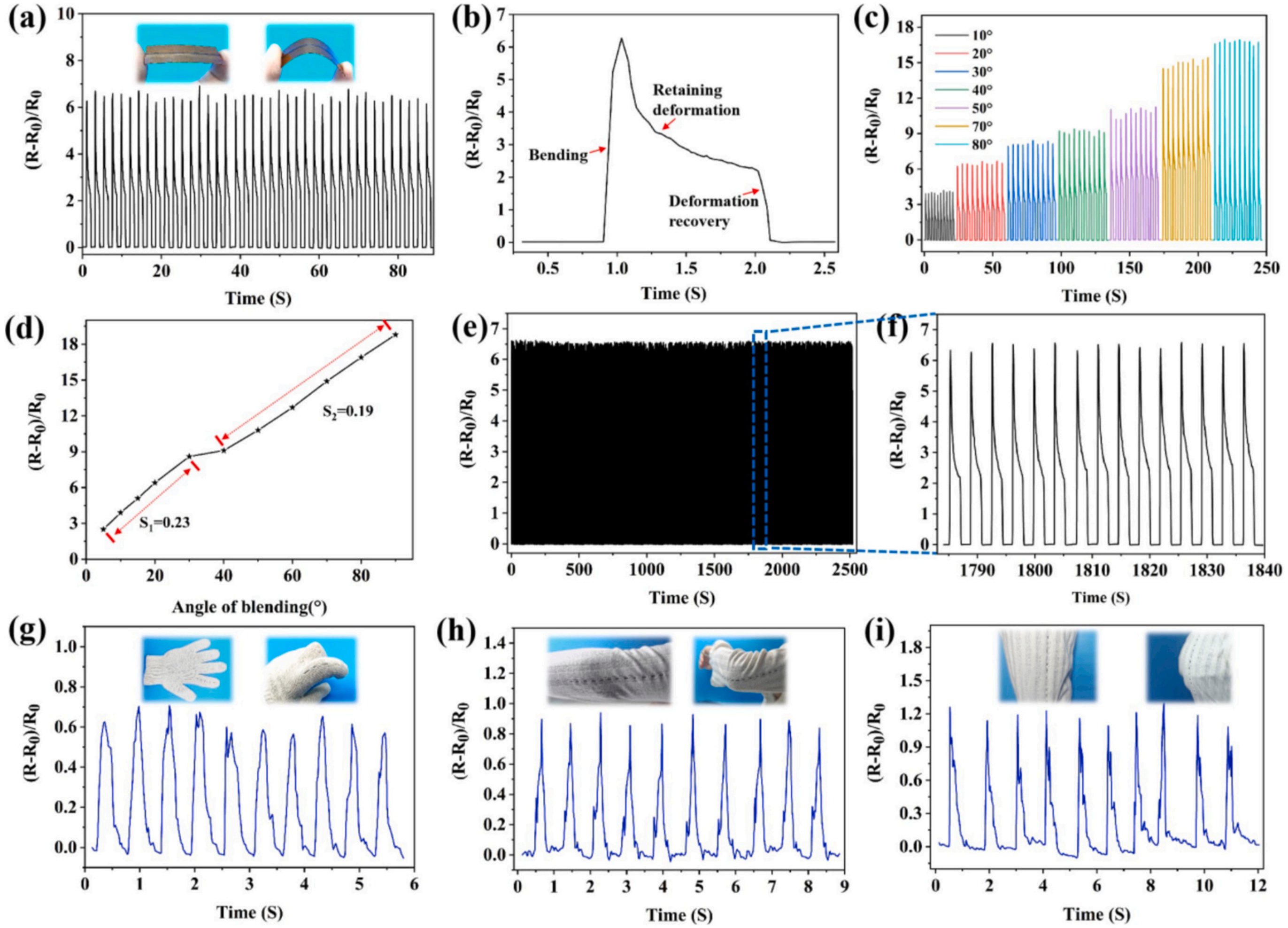

Fig. 7. Sensing properties of the BC/PPy-P macrofiber: (a) sensing properties of fibers against bending deformation; (b) waveforms of fiber resistance change in response to bending deformation; (c) changes in fiber resistance at different bending angles; (d) sensitivity of fiber detection for different bending angles; (e) cyclic performance test of fibers under 1000 cycles of bending deformation; (f) partial enlarged detail of the cyclic test after 800 times; BC/PPy-P fibers embedded in fabrics as strain sensors to monitor movements such as (g) finger bending, (h) arm bending, and (i) leg bending.

3.9. BC/PPy-P macrofibers as resistive strain sensors for human movement monitoring

Furthermore, we utilized the BC/PPy-P macrofiber for human movements to evaluate its potential for practical applications in the field of wearable smart fabrics. First, the macrofiber was sewn into a yarn glove to monitor the bending motion of the fingers. As shown in Fig. 7g, although the resulting generating resistance change was not as large as the previous test results, the bending motion of the finger could still be sensitively captured. In addition, we tested the sensing performance of BC/PPy-P macrofibers sewn into gloves in different humidity environments (Fig. S6). The sensing signal generated by the BC/PPy-P macrofibers decreases with increasing humidity (from 0.69 at 20 % to 0.44 at 85 %). However, the BC/PPy-P macrofibers are still effective in monitoring finger bending motion in high humidity environments, suggesting that it has the potential to monitor motion when the body is sweating. Furthermore, the accurate monitoring of elbow bending (Fig. 7h) and leg bending (Fig. 7i) could be realized by sewing fibers into clothing that corresponded to the body's movement areas. All of these factors indicated that the BC/PPy-P macrofiber had potential applications in the field of sensing due to its fast responsiveness, wide detection range, good stability, and long service life.

4. Conclusions

In summary, we developed an approach to fabricate biodegradable, robust, and conductive macrofibers that consisted of a BC matrix and a conductive material consisting of PPy-P particles. The composite macrofibers as resistive strain sensors exhibited a fast response time and high sensitivity, which could be sewn into clothing to effectively monitor human activity. Moreover, the matrix BC material was capable of being completely biodegraded into harmless glucose and oligosaccharides in the presence of cellulase, while the remaining biocompatible PPy-P particles could be recycled for other uses. Therefore, this work provided a strategy for designing environmentally friendly conductive macrofibers for functional fabrics.

CRediT authorship contribution statement

Zaixian Yuan: Writing – original draft, Visualization, Supervision, Data curation. **Hai Yin:** Data curation. **Min Zheng:** Data curation, Validation. **Xiao Chen:** Formal analysis. **Wei Peng:** Resources, Formal analysis. **Hongfu Zhou:** Visualization, Supervision. **Jun Xing:** Data curation. **Li Wang:** Validation, Supervision, Resources. **Sanming Hu:** Writing – review & editing, Writing – original draft, Resources, Methodology, Investigation.

Declaration of competing interest

The authors declare that they have no known competing financial interests or personal relationships that could have appeared to influence the work reported in this paper.

Acknowledgments

This work was supported by the Hubei University of Science and Technology Doctoral Start-up Fund Project (Grant No. BK202306), Hubei Provincial Natural Science Foundation (2022CFB749), the National Natural Science Foundation of China (52303182), Xianning City Natural Science Foundation (2023ZRKX084), and the Hubei Provincial Education Department Research Young and Middle-aged Talent Fund (Q20222803), Hubei Province Key R&D Plan Big Health Local Special Project (2022BCE042), and the Hubei University of Science and Technology Doctoral Start-up Fund Project (Grant No. 2018-20XB001). We thank LetPub (www.letpub.com.cn) for its linguistic assistance during the preparation of this manuscript.

Appendix A. Supplementary data

Supplementary data to this article can be found online at https://doi.org/10.1016/j.carbpol.2024.122963.

Data availability

The data that has been used is confidential.

References

Chen, N., Wei, W., Ning, N., Wu, H., & Tian, M. (2024). All-polymeric stretchable conductive fiber with versatile intelligent wearable applications via microfluidic spinning technology. *Chemical Engineering Journal, 487*.

Dang, X., Fu, Y., & Wang, X. (2024). A temperature and pressure dual-responsive, stretchable, healable, adhesive, and biocompatible carboxymethyl cellulose-based conductive hydrogels for flexible wearable strain sensor. *Biosensors & Bioelectronics, 246*, Article 115893.

Dong, H. K., Cha, J.-H., Lim, J. Y., Bae, J., Lee, W., Yoon, K. R., Kim, C., Jang, J.-S., Hwang, W., & Kim, I.-D. Colorimetric dye-loaded nanofiber yarn: Eye-readable and weavable gas sensing platform. ACS Nano, 14(12), 16907-16918.

Du, Z., Ai, J., Zhang, X., Ma, Z., Wu, Z., Chen, D., Tao, G., & Su, B. (2020). Stretchable electromagnetic fibers for self-powered mechanical sensing. *Applied Materials Today, 20*, Article 100623.

Fan, W., He, Q., Meng, K., Tan, X., Zhou, Z., Zhang, G., … Wang, Z. L. (2020). Machine-knitted washable sensor array textile for precise epidermal physiological signal monitoring. *Science Advances, 6*, eaay2840.

Fatma, B., Andrabi, S. M., Gupta, S., Verma, V., Kumar, A., Pitsalidis, C., & Garg, A. (2023). Biocompatible, breathable and degradable microbial cellulose based triboelectric nanogenerator for wearable transient electronics. *Nano Energy, 114*.

Goswami, S., Nandy, S., Fortunato, E., & Martins, R. (2023). Polyaniline and its composites engineering: A class of multifunctional smart energy materials. *Journal of Solid State Chemistry, 317*, Article 123679.

Hardman, D., George Thuruthel, T., & Iida, F. (2022). Self-healing ionic gelatin/glycerol hydrogels for strain sensing applications. *NPG Asia Materials, 14*(1).

He, W., Wang, C., Wang, H., Jian, M., Lu, W., Liang, X., … Zhang, Y. (2019). Integrated textile sensor patch for real-time and multiplex sweat analysis. *Science Advances, 5*, Article eaax0649.

Hu, M., Gao, Y., Jiang, Y., Zeng, H., Zeng, S., Zhu, M., Xu, G., & Sun, L. (2021). High-performance strain sensors based on bilayer carbon black/PDMS hybrids. *Advanced Composites and Hybrid Materials, 4*(3), 514–520.

Hu, S., Han, J., Shi, Z., Chen, K., Xu, N., Wang, Y., … Yang, G. (2022). Biodegradable, super-strong, and conductive cellulose macrofibers for fabric-based triboelectric nanogenerator. *Nanomicro Letters, 14*(1), 115.

Hu, S., Zheng, M., Wang, Q., Li, L., Xing, J., Chen, K., … Yang, G. (2022). Cellulose hydrogel-based biodegradable and recyclable magnetoelectric composites for electromechanical conversion. *Carbohydrate Polymers, 298*, Article 120115.

Huo, Y., Guo, D., Yang, J., Chang, Y., Wang, B., Mu, C., … Wen, F. (2022). Multifunctional bacterial cellulose nanofibers/polypyrrole (PPy) composite films for joule heating and electromagnetic interference shielding. *ACS Applied Electronic Materials, 4*(5), 2552–2560.

Jo, Y. J., Kim, S. Y., Hyun, J. H., Park, B., Choy, S., Koirala, G. R., & Kim, T.-I. (2022). Fibrillary gelation and dedoping of PEDOT:PSS fibers for interdigitated organic electrochemical transistors and circuits. *npj Flexible Electronics, 6*(1).

Lee, J., Jeon, S., Seo, H., Lee, J. T., & Park, S. (2021). Fiber-based sensors and energy systems for wearable electronics. *Applied Sciences, 11*(2), 531–558.

Lee, J., Shin, S., Lee, S., Song, J., Kang, S., Han, H., … Lee, T. (2018). Highly sensitive multifilament fiber strain sensors with ultrabroad sensing range for textile electronics. *ACS Nano, 12*(5), 4259–4268.

Li, K., Ni, X., Wu, Q., Yuan, C., Li, C., Li, D., … Ju, A. (2022). Carbon-based fibers: Fabrication, characterization and application. *Advanced Fiber Materials, 4*(4), 631–682.

Li, X., Ma, Y., Li, D., Lu, S., Li, Y., & Li, Z. (2022). Highly stretchable, self-healing, and degradable ionic conductive cellulose hydrogel for human motion monitoring. *International Journal of Biological Macromolecules, 223*(Pt A), 1530–1538.

Li, X., Wan, M., Wei, Y., Shen, J., & Chen, Z. (2006). Electromagnetic functionalized and core-shell micro/nanostructured polypyrrole. *Composites, 110*, 14623–14626.

Liao, J., Luan, P., Zhang, Y., Chen, L., Huang, L., Mo, L., Li, J., & Xiong, Q. (2022). A lightweight, biodegradable, and recyclable cellulose-based bio-foam with good mechanical strength and water stability. *Journal of Environmental Chemical Engineering, 10*(3).

Lin, Z., Yang, J., Li, X., Wu, Y., Wei, W., Liu, J., … Yang, J. (2017). Large-scale and washable smart textiles based on triboelectric nanogenerator arrays for self-powered sleeping monitoring. *Advanced Functional Materials, 28*(1).

Liu, X., Miao, J., Fan, Q., Zhang, W., Zuo, X., Tian, M., … Qu, L. (2022). Recent progress on smart fiber and textile based wearable strain sensors: Materials, fabrications and applications. *Advanced Fiber Materials, 4*(3), 361–389.

Liu, Z., Zhu, T., Wang, J., Zheng, Z., Li, Y., Li, J., & Lai, Y. (2022). Functionalized fiber-based strain sensors: Pathway to next-generation wearable electronics. *Nanomicro Lett, 14*(1), 61.

Lu, H., Zhang, Y., Zhu, M., Li, S., Liang, H., Bi, P., … Zhang, Y. (2024). Intelligent perceptual textiles based on ionic-conductive and strong silk fibers. *Nature Communications, 15*(1), 3289.

Ma, Y., Ouyang, J., Raza, T., Li, P., Jian, A., Li, Z., Liu, H., Chen, M., Zhang, X., Qu, L., Tian, M., & Tao, G. (2021). Flexible all-textile dual tactile-tension sensors for monitoring athletic motion during taekwondo. *Nano Energy, 85*.

Meng, K., Chen, J., Li, X., Wu, Y., Fan, W., Zhou, Z., … Wang, Z. L. (2018). Flexible weaving constructed self-powered pressure sensor enabling continuous diagnosis of cardiovascular disease and measurement of cuffless blood pressure. *Advanced Functional Materials, 29*(5).

Pai, A., Rodriguez-Millan, M., Kini, C. R., Mallya, R., Bekal, C., Yeshwant Nayak, S., & Shenoy, S. B. (2023). Fiber metal laminates for high strain rate applications with layerwise shock impedance tuning. *Scientific Reports, 13*(1), 18474.

Peng, S., Xu, Q., Fan, L., Wei, C., Bao, H., Xu, W., & Xu, J. (2016). Flexible polypyrrole/cobalt sulfide/bacterial cellulose composite membranes for supercapacitor application. *Synthetic Metals, 222*, 285–292.

Qian, S., Wang, X., & Yan, W. (2023). Piezoelectric fibers for flexible and wearable electronics. *Frontiers of Optoelectronics, 16*(1), 3.

Raman, S., & Ravi Sankar, A. (2022). Intrinsically conducting polymers in flexible and stretchable resistive strain sensors: a review. *Journal of Materials Science, 57*(28), 13152–13178.

Sarabia-Riquelme, R., Andrews, R., Anthony, J. E., & Weisenberger, M. C. (2020). Highly conductive wet-spun PEDOT:PSS fibers for applications in electronic textiles. *Journal of Materials Chemistry C, 8*(33), 11618–11630.

Shuai, L., Guo, Z. H., Zhang, P., Wan, J., Pu, X., & Wang, Z. L. (2020). Stretchable, self-healing, conductive hydrogel fibers for strain sensing and triboelectric energy-harvesting smart textiles. *Nano Energy, 78*.

Song, X., Ji, J., Zhou, N., Chen, M., Qu, R., Li, H., … Wei, Y. (2024). Stretchable conductive fibers: Design, properties and applications. *Progress in Materials Science, 144*.

Souri, H., Banerjee, H., Jusufi, A., Radacsi, N., Stokes, A. A., Park, I., … Amjadi, M. (2020). Wearable and stretchable strain sensors: Materials, sensing mechanisms, and applications. *Advanced Intelligent Systems, 2*(8).

Thombal, P. R., & Han, S. S. (2018). Novel synthesis of Lewis and Bronsted acid sites incorporated CS-Fe3O4@SO3H catalyst and its application in one-pot synthesis of tri (furyl)methane under aqueous media. *Biofuel Research Journal, 5*(4), 886–893.

Tian, F., Zhang, Y., Liu, L., Zhang, Y., Shi, Q., Zhao, Q., … Song, X. (2020). Spongy p-toluenesulfonic acid-doped polypyrrole with extraordinary rate performance as durable anodes of sodium-ion batteries at different temperatures. *Langmuir, 36*(49), 15075–15081.

Wang, F., Chen, J., Cui, X., Liu, X., Chang, X., & Zhu, Y. (2022). Wearable ionogel-based fibers for strain sensors with ultrawide linear response and temperature sensors insensitive to strain. *ACS Applied Materials & Interfaces, 14*(26), 30268–30278.

Wang, F., Kim, H.-J., Park, S., Kee, C.-D., Kim, S.-J., & Oh, I.-K. (2016). Bendable and flexible supercapacitor based on polypyrrole-coated bacterial cellulose core-shell composite network. *Composites Science and Technology, 128*, 33–40.

Wang, H., Xue, P., & Zhu, W. L. (2019). An integrated numerical method to predict the strain sensing behavior of flexible conductive fibers under electric–thermal conditions. *Journal of Materials Engineering and Performance, 28*(6), 3309–3319.

Wang, J., Tavakoli, J., & Tang, Y. (2019). Bacterial cellulose production, properties and applications with different culture methods - A review. *Carbohydrate Polymers, 219*, 63–76.

Wang, J., Wang, L., Zhang, Y., Pan, J., Li, S., Sun, X., … P., H. (2018). Weaving sensing fibers into electrochemical fabric for real-time health monitoring. *Advanced Functional Materials, 28*(42), Article 1804456.

Wang, S., Jiang, F., Xu, X., Kuang, Y., Fu, K., Hitz, E., & Hu, L. (2017). Super-strong, super-stiff macrofibers with aligned, long bacterial cellulose nanofibers. *Advance Materials, 29*(35).

Wang, T., Ouyang, Z., Wang, F., & Liu, Y. (2020). A review on graphene strain sensors based on fiber assemblies. *SN Applied Sciences, 2*(5).

Wang, X., Sun, H., Yue, X., Yu, Y., Zheng, G., Dai, K., Liu, C., & Shen, C. (2018). A highly stretchable carbon nanotubes/thermoplastic polyurethane fiber-shaped strain sensor with porous structure for human motion monitoring. *Composites Science and Technology, 168*, 126–132.

Wang, Z., Chen, C., Fang, L., Cao, B., Tu, X., Zhang, R., Dong, K., Lai, Y.-C., & Wang, P. (2023). Biodegradable, conductive, moisture-proof, and dielectric enhanced cellulose-based triboelectric nanogenerator for self-powered human-machine interface sensing. *Nano Energy, 107*.

Wu, S., Liu, Z., Gong, C., Li, W., Xu, S., Wen, R., … Yan, Y. (2024). Spider-silk-inspired strong and tough hydrogel fibers with anti-freezing and water retention properties. *Nature Communications, 15*(1), 4441.

Xu, J., Zhu, L., Bai, Z., Liang, G., Liu, L., Fang, D., & Xu, W. (2013). Conductive polypyrrole–bacterial cellulose nanocomposite membranes as flexible supercapacitor electrode. *Organic Electronics, 14*(12), 3331–3338.

Zhang, J., Hu, S., Shi, Z., Wang, Y., Lei, Y., Han, J., … Wang, Z. L. (2021). Eco-friendly and recyclable all cellulose triboelectric nanogenerator and self-powered interactive interface. *Nano Energy, 89*.

Zhang, R., Pan, P., Dai, Q., Yang, X., Yang, Z., Wei, J., Liu, J., & Yuan, Q. (2018). Sensitive and wearable carbon nanotubes/carbon black strain sensors with wide linear ranges for human motion monitoring. *Journal of Materials Science: Materials in Electronics, 29*(7), 5589–5596.

Zheng, L., Zhu, M., Wu, B., Li, Z., Sun, S., & Wu, P. (2021). Conductance-stable liquid metal sheath-core microfibers for stretchy smart fabrics and self-powered sensing. *Science Advances, 7*, Article eabg4041.